Comparison of Modular Stator 1-phase per Module with Switched Reluctance Motor

Syed Muhammad Naufal Syed Othman
University Tun Hussein Onn Malaysia, Malaysia
smnaufal@gmail.com (corresponding author)

Erwan Sulaiman
University Tun Hussein Onn Malaysia, Malaysia
erwan@uthm.edu.my

Nur Afiqah Mostaman
University Tun Hussein Onn Malaysia, Malaysia
afiqahmostaman98@gmail.com

Roshada Ismail
University Tun Hussein Onn Malaysia, Malaysia
roshadaismail98@gmail.com

Mahyuzie Jenal
University Tun Hussein Onn Malaysia, Malaysia
mahyuzie@uthm.edu.my

Received: 19 February 2024 | Revised: 26 March 2024 | Accepted: 28 March 2024

 DOI: https://doi.org/10.48084/etasr.7101

ABSTRACT

Conventional motors have the advantage of robustness, high torque output capability, and power performance compared to modular motors. However, traditional motor structure inhibits fault tolerance. For that reason, this paper proposes the structure of a modular stator. It focuses on the performance of modular stator outer rotor flux switching permanent magnet motor (MSOR-FSPM) and Segmental Stator Hybrid Excitation Switched Reluctance Motor (SS-HESRM) by simulation using 2D-FEA in no-load and load conditions. Based on the results, the maximum flux linkage of MSOR-FSPM is 0.02 Wb and 0.05 Wb for SS-HESRM. The average torque output for MSOR-FSPM at maximum armature density is 108.43 Nm and 45.26 Nm for SS-HESRM. Therefore, the torque density for MSOR-FSPM and SS-HESRM is 3.78 Nm/kg and 10.63 Nm/kg, respectively. As for the conclusion, a modular stator motor is capable of inherent fault tolerance compared to a conventional motor structure. Moreover, a modular stator motor produces a higher torque and power density because of the low iron core and optimum flux linkage.

Keywords-flux-switching; fault-tolerance motor; modular stator; permanent magnet

I. INTRODUCTION

The types of Alternating Current (AC) motors are Induction Motor (IM), Switch-Reluctance Motor (SRM), and Permanent Magnet (PM) motor. IM has the advantages of low cost and simple motor controller, which is used widely in low torque and lightweight applications with 70-80% efficiency [1, 2]. In contrast to IM, the independent concentrated phase winding is the characteristic and advantage of SRM, which acts as a fault-tolerant motor. However, both motors are considered to be low-torque performance motors compared to PM-based motors. This is because IM and SRM have similarities depending on reluctance torque, and have been shown to have low output torque compared to magnetic torque in PM-based motors [3-5].

The application of PM in the motor can be categorized into Surface-Mounted PM Motor (SPM), Interior PM Motor (IPM), Flux-Switching Motor (FSPM), and Hybrid-Excitation Flux-Switching Motor (HEFSM) [6, 7]. Based on the application of PM, it can be incorporated inside or on the surface of the rotating structure [8, 9]. IPM and SPM have been commonly used in industrial and domestic appliances due to their high efficiency of 80-93% with a wide power range against speed range, and have been explicitly associated with electric

vehicles for their traction appliances [10]. Moreover, due to its high power rating, SPM is developed for industrial applications such as robotic arms, electrical tools, and auxiliary power units [11]. An example of the advanced and complicated designs of SPM utilizing a skew structure in industrial applications is the V-type skew and X-type skew [12]. Another type of PM-based motor is the FSPM, which is an efficient development in drive systems and attracts the researchers' interest due to its high torque density, higher efficiency, and rigid rotor assembly compared to IPM and SPM [13, 14]. Furthermore, the improvement of FSPM in high-speed range generators is due to the compelling part of PM demagnetization relief in high-speed operation [16].

Early development of modular radial-field stator design of PM synchronous machine was designed for grid-connected wind turbines and with power ratings from 100 kW to more than 1 MW since 1996 [16]. Modular stator arrangement creates a low reactance but high efficiency for PMSM due to the concentrated flux with a short path. A modular E-core stator PMFSM was designed in [17] as a simple, robust rotor structure with high torque density. Besides that, it was shown that modular stators with higher than stator tooth numbers degrade the electromagnetic performance due to lower winding factor and flux defocusing effect than conventional stator motors [18].

Therefore, this paper will discuss, analyze, and compare the performance between SS-HESRM and MSOR FSPM. Both designs share the typical characteristics of the modular stator with a structure of 1-phase/ module, where the SS-HESRM is a type of SRM integrated with PM, and MSOR FSPM is an outer rotor FSPM. This paper examines the performance in terms of flux linkage, average torque at various current loads, and finally, each design's torque density and power density. The significance of the modular stator structure and the characteristics of higher torque density per copper loss than its counterpart is highlighted in the conclusion.

II. MOTOR TOPOLOGY AND OPERATING PRINCIPLE

The topologies of the three-phase stator MSOR-FSPM and SS-HESRM with the configuration of 1-phase per module stator are illustrated in Figures 1 and 2. The circumferential flux of the MSOR FSPM includes the stator core, stator armature coil, and PM at the inner part compared to the conventional outer circumferential flux for the SS-HESRM. Unlike the traditional stator structure of both designs, MSOR FSPM and SS-HESRM have an air gap between each modular stator where there is no flux linkage between the stator modules. The structure of the modular stator is different for MSOR FSPM and SS-HESRM. There are two armature windings with two directions in SS-HESRM, while only one is in MSOR FSPM. Despite that, both designs have a PM on each stator module as a magnetic flux in which PM is sandwiched between two C-shaped iron stator cores for MSOR FSPM compared to a single C-shaped modular iron stator core, and each stator pole is wound with armature for SS-HESRM. The phase of armature winding in each modular stator for both designs is shown in Figures 1 and 2. As for the rotor structure, both designs are a stack of laminated iron cores that become a single rotor part with a different number of poles for each design. The topology for MSOR FSPM is 6-Slot/ 20-Pole and 12-Slot/ 10-Pole for SS-HESRM [19].

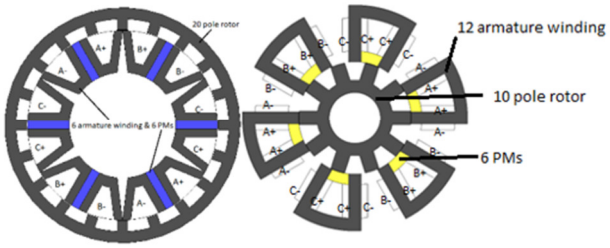

Fig. 1. Machine topology with armature winding.

Figure 2 shows the operating principle of SS-HESRM in one segment without armature current injection and with current injection. When the armature coils are not excited, I = 0 A, and the flux generated by PM is only circulated through the U-core stator iron segments and does not connect with the rotor pole and does not pass the airgap, as shown in Figure 2(a). The flux path is shown in Figure 2(b) and (c) when the armature coils are excited at aligned and unaligned rotor positions. Based on the flux generated by PM (blue arrow) in the opposite direction and compared to the armature coil excitation (red arrow), the flux from the excited coil cancels the PM flux. Therefore, when the armature coils are excited with low current, the maximum flux in the stator pole is negative. Likewise, if high currents are injected and excited by the armature coils, the total flux is positive in the stator pole. It is different at the rotor part and air gap because the PM and excited coil flux are summed together in the same direction. This flux is higher than that in the field-excited coil only type of motor, such as IM, because there is no PM flux. The airgap reluctance at aligned and unaligned positions is different, which varies the flux value in the stator coil and pole [20].

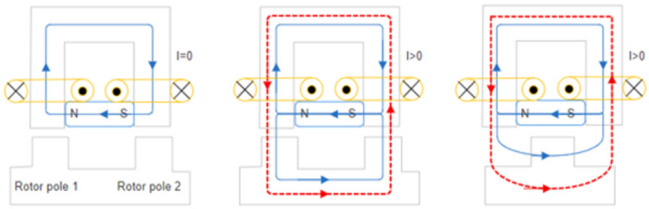

(a) (b) (c)

Fig. 2. Machine topology with armature winding.

III. DESIGN SPECIFICATION AND METHODOLOGY

The design specification and parameters restriction of MSOR FSPM and SS-HESRM are listed in Tables I and II. The 2D-FEA of both designs is divided into two parts, which involves various magnetic flux analyses in no-load conditions and torque performance at increasing armature current density (J_A). For the final analysis, performance verification is carried out by comparing the MSOR FSPM and SS-HESRM results in terms of maximum magnetic flux linkage, flux line, flux

strengthening profiles, back-emf analysis, and torque performance at various armature densities [21].

TABLE I. DESIGN MATERIALS OF MSOR FSPM AND SS-HESRM

Item	Material	Density (kg/m^3)
Stator and Rotor	Soft Magnetic Steel	7600
Permanent Magnet	(35H250)	7550
Armature coil	Neomax-35 AHκ	8960

TABLE II. DESIGN SPECIFICATIONS OF MSOR FSPM AND SS-HESRM

Specifications	MSOR FSPM	SS-HESRM
Number of phases	1-phase/ module	
Speed	1200 rpm	
Pole numbers	20	10
Stator slot	6	12
Outer diameter	264 mm	
Stack length	70 mm	
Rotor radius	132 mm	65.5 mm
Airgap	0.5 mm	
Magnet width	9.4 mm	20 mm
Stator width	9.4 mm	14.7 mm
Rotor width	12 mm	17.12 mm

The total weight coefficient of the motors consists of three components: iron core, PM, and copper winding, as shown in (1):

$$W_{motor} = W_{ic} + W_{PM} + W_{cw} \quad (1)$$

Based on NEOMAX-35AH, a type of neodymium magnet, the weight of the PM can be calculated as:

$$W_{PM} = \text{No.of } PM \times Vol_{PM} \times 7550 \text{ kgm}^{-3} \quad (2)$$

The weight of copper winding, W_{cw} is based on the wire length, L and the midpoints between a pair of slots, with the midpoint of the width of single slot. Therefore, it can be calculated as in (3):

$$L = H_1 + H_2 + E_1 + E_2 \quad (3)$$

$$E = \pi r_3 \quad (4)$$

$$L = 2\text{H} + 2\pi r_3 \quad (5)$$

$$W_{cw} = Vol_{cw} \times 8960 \text{ kgm}^{-3} \quad (6)$$

The detailed weights of MSOR FSPM and SS-HESRM are listed in Table III .

TABLE III. DETAIL WEIGHT ESTIMATION

Parts	Estimated Weight (kg)	
	MSOR FSPM	SS-HESRM
Rotor iron	6.88	3.75
Stator iron	6.08	8.57
Permanent magnet	1.39	0.92
Copper winding	1.07	0.36
Total weight	15.42	13.60

IV. RESULTS AND DISCUSSION

A. Flux Interaction between PM and Armature Coil

The interactions between PM flux, armature coil, and PM flux with armature coil flux characteristics are investigated to determine the resulting flux. However, a sinusoidal distribution of flux linkage in space is necessary to avoid losses. The resultant flux in Figure 3 and Figure 4 depicts the operating principle, where the rotating motion and the flux interaction create angle shifting. The resulting flux of MSOR FSPM in Figure 3 shows a sinusoidal phase shift of angle -8° while SS-HESRM is precisely at the correct angle [22]. The graph verifies that the maximum resultant flux of MSOR FSPM is 0.021 Wb which is lower than the AC flux only by 0.031 Wb. In this context, the AC flux cancels out the magnetic field on the outer side [23]. However, the result is different for SS-HESRM in Figure 4, where the maximum resultant flux, 0.052 Wb, is higher by combining both PM and AC magnetic fluxes. The resultant flux of MSOR FSPM is more sinusoidal than SS-HESRM, where the amplitude is unbalanced, affecting the peak-to-peak ratio to -0.14.

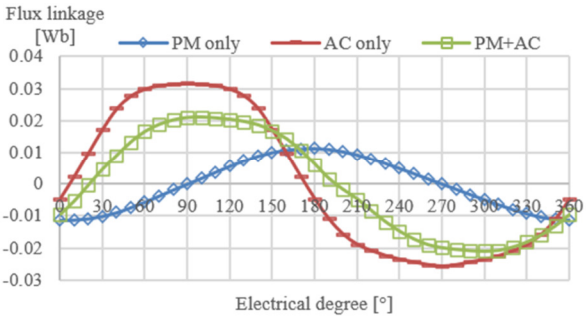

Fig. 3. Resultant flux for MSOR FSPM.

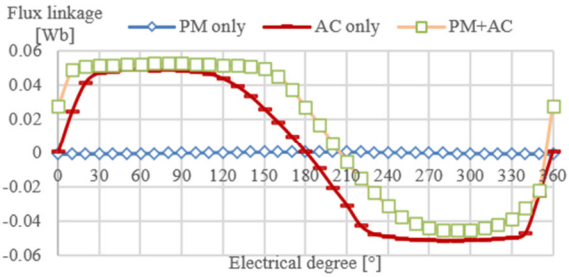

Fig. 4. Resultant flux for SS-HESRM.

B. Maximum Flux Linkage

The magnetic flux of both designs is compared to a hybrid excitation motor, which has a Field-Excitation (FE) [24]. Therefore, to study the flux strengthening and weakening of a PM motor, analysis is carried out from 0 Arms/mm^2 to a maximum of 30 Arms/mm^2 as shown in Figure 5. Obviously, the flux linkage of MSOR FSPM and SS-HESRM starts with a value of 0.013 Wb and 0.030 Wb and strengthens with increasing J_A and starts to weaken when it reaches a maximum of 30 Arms/mm^2 which stops at 0.021 Wb and 0.052 Wb, respectively [25]. Based on Figure 5, the difference of

maximum flux is about 1.5 times at 30 Arms/mm^2 and the significant difference in flux performance is due to the magnetic flux route factor, where the SS-HESRM design has shorter magnetic path [27].

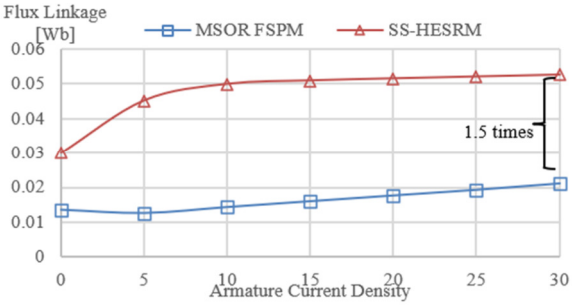

Fig. 5. Flux Linkage with various armature current densities.

C. Back EMF Evaluation

The evaluation of back EMF is conducted at no load condition and with a revolving motion of both motors at a rated velocity of 1200 rpm. Back EMF analysis determines the voltage induced in an electric motor wherein the armature and the magnet field from the PMs may cause relative motion [27]. Figure 6 compares back EMF between the harmonics and the fundamental frequency (F). In Figure 6 MSOR FSPM has a maximum value of 27.12 V at 80° angle and a minimal value of -23.86 V at 290°. Meanwhile, SS-HESRM has a maximum value of 6.18 V at 100° and a minimal value of -6.19 V at 320°. Although the amplitude of MSOR FSPM is remarkably larger than SS-HESRM's, the no-load phases back EMF of both design waveforms are symmetrical, and the amplitude corresponds to the fundamental. The harmonics in the back EMF waveform of MSOR FSPM are fundamentally higher, increasing the average torque and torque ripple due to the cogging torque [28].

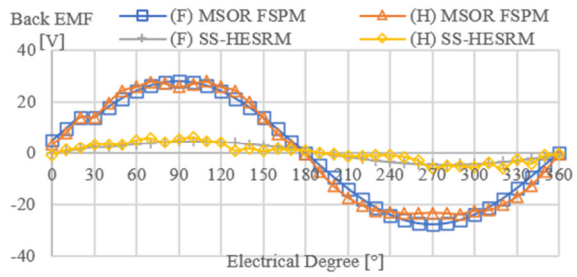

Fig. 6. Back EMF against fundamentals.

D. Cogging Torque Analysis

The generation of cogging torque occurs where the interference between the magnetic field of the PM and stator slots affects the changes in the reluctance that depends on the rotor pole position. This phenomenon will occur when the motor has an air gap, which raises the flux linkage and disrupts the torque performance. Therefore, a low cogging torque is the best for motor conditions compared to a high cogging torque, which will induce motor vibration. Figure 7 compares the cogging torque performance for MSOR FSPM and SS-HESRM. Figure 7 shows 7.05 Nm peak-to-peak cogging torque for MSOR FSPM and 0.001 Nm for SS-HESRM. The difference in cogging torque values can be explained by the number of stator poles, which is 24 for the MSOR FSPM and 12 for the SS-HESRM. High flux linkage from the PM and airgap affects the poor torque performance caused by the high cogging torque. To minimize the cogging torque, several methods such as chamfering and notching can be applied to the design [29, 30]. The high cogging torque of MSOR FSPM is correlated with harmonics and back EMF as explained above.

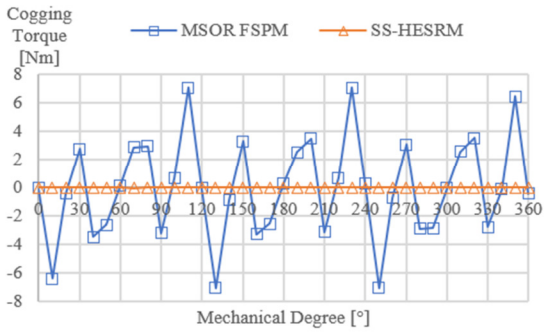

Fig. 7. Cogging torque analysis.

E. Average Torque Performance

Figure 8 illustrates the torque performance at various J_A for MSOR FSPM and SS-HESRM. The increase in torque for both designs can be considered linearly to J_A. At the peak, J_A, MSOR FSPM, and SS-HESRM designs give output torque of 108.4 Nm and 45.3 Nm, respectively. To simplify, the MSOR FSPM design has higher torque output than SS-HESRM, although the flux linkage gives the opposite results [19]. The average torque of MSOR FSPM is 2.4 times that of SS-HESRM, and this proves that a flux-switching machine generates high torque output performance due to flux-switching generated at the inner modular stator core with a high number of rotor poles. Moreover, the torque ripple and vibration affect the average torque output of SS-HESRM [9].

MSOR FSPM is typically a flux switching machine which has lower losses compared to SRM, and this results in higher torque output. Moreover, MSOR FSPM utilizes a unique flux control mechanism where the magnetic flux in the machine can be effectively modulated. This allows for better utilization of the available magnetic flux and enables higher torque generation. An advanced control strategy can optimize the machine operation based on parameters such as speed, load conditions, and requirements. As seen in Figure 8, it has been proven that MSOR FSPM and SS-HESRM can be applied to various three-phase applications since the torque increases linearly [26, 31].

F. Torque and Power Performance

Based on Table IV, the torque density of SS-HESRM is lower than that of MSOR-FSPM. The drawbacks of SRM are proven to be low torque density, high torque ripple, high acoustic noise, and vibration limit to industrial applications [32]. Although both motor designs have the same outer

diameter with a modular stator structure, which is considered to reduce the overall volume of the motor, the torque and power density differ. The difference in weight is 1.82 kg, but the average torque output is enormous, which makes the torque density for SS-HESRM 3.33 Nm/kg while for MSOR FSPM it is 7.03 Nm/kg. The torque and power difference percentage between the motors is approximately 58.24%, where the power density for MSOR FSPM is 8.44 kW/kg, which is higher than SS-HESRM, which is 3.99 kW/kg.

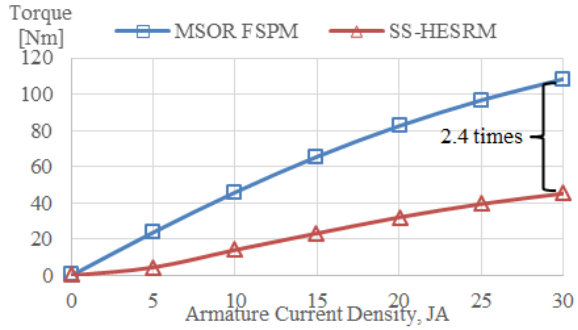

Fig. 8. Average torque relative to armature current density.

Accordingly, the torque and power density of modular stator structures are higher than those of stators with salient core structures at the same conditions and speed. Moreover, modular stator structures are able to optimize the magnetic material and iron cores by exhibiting high flux-carrying capability, thereby achieving greater power density than conventional structures [33, 34]. Finally, the design and analysis of 12-Slot/ 20-Pole MSOR FSPM and 6-Slot/10-Pole SS-HESRM have been presented. Both motors have been successfully designed and analyzed using JMAG Designer version 18, 2D FEA. The results of flux strengthening, back-EMF, cogging torque, average torque at various loads, and torque density have been compared for performance verification.

TABLE IV. TORQUE AND POWER DENSITY

Performance	SS-HESRM	MSOR-FSPM
Estimated weight (kg)	13.6	15.42
Avg. torque (Nm)	45.26	108.4
Torque density (Nm/kg)	3.33	7.03
Power (kW)	54.31	130.08
Power density (kW/kg)	3.99	8.44

V. CONCLUSIONS

In conclusion, MSOR FSPM achieves a higher average torque of 108.4 Nm, and torque density of 7.03 Nm/kg, compared to the average torque of SS-HESRM, which is 45.26 Nm, and torque density of 3.33 Nm/kg. Moreover, the power density of MSOR FSPM, which is 8.44 kW/kg, is higher than SS-HESRM's which is 3.99 kW/kg. The contribution of the current work is the performance of the motor in terms of torque density and power density of the flux switching motor compared to the switched reluctance motor. Although MSOR FSPM has a higher volume of iron core for the stator and rotor, which increases the overall mass by 1.82 kg compared to SS-HESRM, the difference of the average torque is 63.14 Nm and has 2.11 times higher torque density. Besides, it has been proven that the higher torque and power density in modular stator motors are significant because the flux distribution is evenly distributed and flux switching focuses on the stator-rotor pole contrary to the conventional SRM and OR-FSPM [19, 35].

ACKNOWLEDGMENT

This research was supported by Ministry of Higher Education (MOHE) through Fundamental Research Grant Scheme (FRGS) (FRGS/1/2023/TK08/UTHM/01/1) and Universiti Tun Hussein Onn Malaysia (UTHM) through Tier 1 (vot Q173)

REFERENCES

[1] L. A. Pereira, G. Nicol, L. F. A. Pereira, and M. Perin, "Induction distribution of five-phase induction machines under open-phase fault," *ISA Transactions*, vol. 96, pp. 468–478, Jan. 2020, https://doi.org/10.1016/j.isatra.2019.06.001.

[2] A. T. Radhi, "Detection and localization of asymmetry in stator winding of three phase induction motors based on fuzzy neural petri net," *Journal of Engineering Science and Technology*, vol. 15, no. 4, pp. 2379–2394, 2020.

[3] P. T. Hieu, D.-H. Lee, and J.-W. Ahn, "High Speed Segmental Stator Type 4/3 SRM: Design, Analysis, and Experimental Verification," *Journal of Electrical Engineering and Technology*, vol. 12, no. 5, pp. 1864–1871, Sep. 2017, https://doi.org/10.5370/JEET.2017.12.5.1864.

[4] A. Kumar, S. Marwaha, and M. S. Manna, "Torque Ripple Mitigation of Switched Reluctance Motor for Water Pumping Applications At Off-Grid Locations," *Journal of Engineering Science and Technology*, vol. 18, no. 1, pp. 147–166, Feb. 2023.

[5] D. B. Minh, L. D. Hai, T. L. Anh, and V. D. Quoc, "Electromagnetic Torque Analysis of SRM 12/8 by Rotor/Stator Pole Angle," *Engineering, Technology & Applied Science Research*, vol. 11, no. 3, pp. 7187–7190, Jun. 2021, https://doi.org/10.48084/etasr.4168.

[6] E. Sulaiman, M. Z. Ahmad, Z. A. Haron, and T. Kosaka, "Design studies and performance of HEFSM with various slot-pole combinations for HEV applications," in *2012 IEEE International Conference on Power and Energy (PECon)*, Kota Kinabalu, Malaysia, Dec. 2012, pp. 424–429, https://doi.org/10.1109/PECon.2012.6450250.

[7] S. M. N. S. Othman and E. Sulaiman, "Design study of 3-phase field-excitation flux switching motor with outer-rotor configuration," in *2014 IEEE 8th International Power Engineering and Optimization Conference (PEOCO2014)*, Langkawi, Malaysia, Mar. 2014, pp. 330–334, https://doi.org/10.1109/PEOCO.2014.6814449.

[8] O. Ocak, M. Onsal, and M. Aydin, "Development of a 7.5kW High Speed Interior Permanent Magnet Synchronous Spindle Motor for CNC Milling Machine," in *2018 XIII International Conference on Electrical Machines (ICEM)*, Greece, Sep. 2018, pp. 704–709, https://doi.org/10.1109/ICELMACH.2018.8506701.

[9] S. G. Lee, K.-S. Kim, J. Lee, and W. H. Kim, "A Novel Methodology for the Demagnetization Analysis of Surface Permanent Magnet Synchronous Motors," *IEEE Transactions on Magnetics*, vol. 52, no. 3, pp. 1–4, Mar. 2016, https://doi.org/10.1109/TMAG.2015.2490203.

[10] J. Dong, Y. Huang, L. Jin, and H. Lin, "Comparative Study of Surface-Mounted and Interior Permanent-Magnet Motors for High-Speed Applications," *IEEE Transactions on Applied Superconductivity*, vol. 26, no. 4, pp. 1–4, Jun. 2016, https://doi.org/10.1109/TASC.2016.2514342.

[11] C. He and T. Wu, "Analysis and design of surface permanent magnet synchronous motor and generator," *CES Transactions on Electrical Machines and Systems*, vol. 3, no. 1, pp. 94–100, Mar. 2019, https://doi.org/10.30941/CESTEMS.2019.00013.

[12] M. Jenal, S. M. N. S. Othman, and E. Sulaiman, "Study of permanent magnet configuration in alternate circumferential and radial flux

permanent magnet flux switching machines (AlCiRaF-PMFSM)," *IOP Conference Series: Materials Science and Engineering*, vol. 917, no. 1, Sep. 2020, Art. no. 012004, https://doi.org/10.1088/1757-899X/917/1/012004.

[13] M. F. Mohd Ab HaliM and E. SulaiMan, "Permanent Magnet Flux Switching Torque Performance Indicator," *El-Cezeri Fen ve Mühendislik Dergisi*, Feb. 2021, https://doi.org/10.31202/ecjse.842739.

[14] Rupam, S. Marwaha, and A. Marwaha, "Finite Element Based Parametric Analysis of Pmsm for Electric Vehicle Applications," *Journal of Engineering Science and Technology*, vol. 18, no. 1, pp. 735–750, Feb. 2023

[15] N. A. Mostaman, E. Sulaiman, M. Jenal, and I. A. Somroo, "Initial Design of Free energy magnetic generator (FEMG)," *IOP Conference Series: Earth and Environmental Science*, vol. 1261, no. 1, Dec. 2023, Art. no. 012005, https://doi.org/10.1088/1755-1315/1261/1/012005.

[16] E. Spooner, A. C. Williamson, and G. Catto, "Modular design of permanent-magnet generators for wind turbines," *IEE Proceedings - Electric Power Applications*, vol. 143, no. 5, 1996, Art. no. 388, https://doi.org/10.1049/ip-epa:19960434.

[17] J. T. Chen and Z. Q. Zhu, "Winding Configurations and Optimal Stator and Rotor Pole Combination of Flux-Switching PM Brushless AC Machines," *IEEE Transactions on Energy Conversion*, vol. 25, no. 2, pp. 293–302, Jun. 2010, https://doi.org/10.1109/TEC.2009.2032633.

[18] G. J. Li, Z. Q. Zhu, W. Q. Chu, M. P. Foster, and D. A. Stone, "Influence of Flux Gaps on Electromagnetic Performance of Novel Modular PM Machines," *IEEE Transactions on Energy Conversion*, vol. 29, no. 3, pp. 716–726, Sep. 2014, https://doi.org/10.1109/TEC.2014.2312429.

[19] J. Zhao, Y. Zheng, C. Zhu, X. Liu, and B. Li, "A Novel Modular-Stator Outer-Rotor Flux-Switching Permanent-Magnet Motor," *Energies*, vol. 10, no. 7, Jul. 2017, Art. no. 937, https://doi.org/10.3390/en10070937.

[20] W. Ding, S. Yang, and Y. Hu, "Development and Investigation on Segmented-Stator Hybrid-Excitation Switched Reluctance Machines With Different Rotor Pole Numbers," *IEEE Transactions on Industrial Electronics*, vol. 65, no. 5, pp. 3784–3794, May 2018, https://doi.org/10.1109/TIE.2017.2760846.

[21] S. M. N. S. Othman, E. Sulaiman, and M. Jenal, "Analytical Design Structure of New Segmental Stator Permanent Magnet Flux Switching Motor," *IOP Conference Series: Materials Science and Engineering*, vol. 917, no. 1, Sep. 2020, Art. no. 012003, https://doi.org/10.1088/1757-899X/917/1/012003.

[22] H. Ali *et al.*, "Design and analysis of double stator HE-FSM for aircraft applications," *International Journal of Power Electronics and Drive Systems (IJPEDS)*, vol. 12, no. 1, Mar. 2021, Art. no. 51, https://doi.org/10.11591/ijpeds.v12.i1.pp51-58.

[23] A. Habib, H. S. Che, E. Sulaiman, and M. Tousizadeh, "A comparative study on the performance of SSDR coreless AFPM generators with conventional and Halbach magnet arrays," *Journal of Engineering Research*, vol. 9, no. 4A, Dec. 2021, https://doi.org/10.36909/jer.8811.

[24] S. K. Rahimi, Z. Ahmad, E. Sulaiman, E. Mbadiwe I, and S. M. N. S. Othman, "Performance Analysis of 12Slot with Various Rotor Pole Numbers HE-FSM for HEV Application," *International Journal of Power Electronics and Drive Systems (IJPEDS)*, vol. 8, no. 4, Dec. 2017, Art. no. 1886, https://doi.org/10.11591/ijpeds.v8.i4.pp1886-1893.

[25] W. Ding, S. Yang, and Y. Hu, "Performance Improvement for Segmented-Stator Hybrid-Excitation SRM Drives Using an Improved Asymmetric Half-Bridge Converter," *IEEE Transactions on Industrial Electronics*, vol. 66, no. 2, pp. 898–909, Feb. 2019, https://doi.org/10.1109/TIE.2018.2833034.

[26] M. F. Omar, E. Sulaiman, H. A. Soomro, M. A. A. Rahim, and J. A. Rani, "Optimal performances of single-phase field excitation flux-switching machine using segmental rotor and non-overlap windings," *Journal of Engineering Science and Technology*, vol. 14, no. Special Issue on SU18, pp. 273–285, Feb. 2019.

[27] W. Hua, P. Su, M. Tong, and J. Meng, "Investigation of a Five-Phase E-Core Hybrid-Excitation Flux-Switching Machine for EV and HEV Applications," *IEEE Transactions on Industry Applications*, vol. 53, no. 1, pp. 124–133, Jan. 2017, https://doi.org/10.1109/TIA.2016.2608324.

[28] G. Zhao and W. Hua, "Comparative Study Between a Novel Multi-Tooth and a V-Shaped Flux-Switching Permanent Magnet Machines," *IEEE Transactions on Magnetics*, vol. 55, no. 7, pp. 1–8, Jul. 2019, https://doi.org/10.1109/TMAG.2019.2900749.

[29] M.-H. Hwang, H.-S. Lee, and H.-R. Cha, "Analysis of Torque Ripple and Cogging Torque Reduction in Electric Vehicle Traction Platform Applying Rotor Notched Design," *Energies*, vol. 11, no. 11, Nov. 2018, Art. no.3053, https://doi.org/10.3390/en11113053.

[30] J. A. Rani and E. Sulaiman, "Performance analysis of cogging torque reduction technique on hybrid flux switching motor," *Journal of Engineering Science and Technology*, vol. 14, no. Special Issue on SU18, pp. 179–190, Feb. 2019.

[31] K. Zhang, G. J. Li, Z. Q. Zhu, and G. W. Jewell, "Investigation on Contribution of Inductance Harmonics to Torque Production in Multiphase Doubly Salient Synchronous Reluctance Machines," *IEEE Transactions on Magnetics*, vol. 55, no. 4, pp. 1–10, Apr. 2019, https://doi.org/10.1109/TMAG.2019.2899803.

[32] W. Ding, Y. Hu, Q. Ze, X. Liu, and Y. Liu, "A novel modular E-core stators and segmental rotors switched reluctance machine for electric vehicles," in *2014 Ninth International Conference on Ecological Vehicles and Renewable Energies (EVER)*, Monte-Carlo, Mar. 2014, pp. 1–8, https://doi.org/10.1109/EVER.2014.6844124.

[33] D. Wang, X. Du, D. Zhang, and X. Wang, "Design, Optimization, and Prototyping of Segmental-Type Linear Switched-Reluctance Motor With a Toroidally Wound Mover for Vertical Propulsion Application," *IEEE Transactions on Industrial Electronics*, vol. 65, no. 2, pp. 1865–1874, Feb. 2018, https://doi.org/10.1109/TIE.2017.2740824.

[34] M. I. Enwelum, L. C. Peng, and E. B. Sulaiman, "Sustainable high torque for electric scooter propulsion using permanent magnet flux switching machine technology," vol. 14, no. Special Issue on SU18, pp. 286–299, Feb. 2019.

[35] W. Ding, S. Yang, Y. Hu, S. Li, T. Wang, and Z. Yin, "Design Consideration and Evaluation of a 12/8 High-Torque Modular-Stator Hybrid Excitation Switched Reluctance Machine for EV Applications," *IEEE Transactions on Industrial Electronics*, vol. 64, no. 12, pp. 9221–9232, Dec. 2017, https://doi.org/10.1109/TIE.2017.2711574.